Supplementary Information for

How Clathrin-Coated Pits Control Nanoparticle Avidity for Cells

Oliver Zimmer, Achim Goepferich

Email: achim.goepferich@ur.de

This Supplementary Information includes:

Supplementary Text
Figures S1 to S5
Tables S1 to S2
SI References

Supplementary Text

Detailed derivation of *δ*-sensitive binding model. The key conceptual approach of our theoretical considerations is the correction of the nanoparticle's valency for the particles wrapping fraction.

$$N = \delta N_t + 1$$

<div align="right">(1)</div>

In equation (1) N_t is the total amount of ligands attached to the respective nanoparticle and δ expressing the wrapping fraction ranging from 0 (no wrapping) to 1 (total wrapping of the particle). The term +1 denotes a single ligand-receptor bond that can be formed regardless of the wrapping fraction (i.e., on an entirely flat membrane).

With δ expressed as the ratio of membrane area where gaussian curvature K_m of the membrane is in good correspondence to the curvature k_{NP} of the given spherical nanostructure A_m ($K_m \approx k_{NP}$) and the nanostructures surface area O_{NP} (Eq. 5 in the main text), we yield a factor describing the wrapping fraction. A first definition for the degree of wrapping of a particle at a membrane was introduced by Deserno *et al.* (1). Later, Agudo-Canalejo *et al.* (2) introduced a degree of invagination that corresponds to the one we employed. The wrapping fraction is based on the surface area on the membrane where particle curvature k_{NP} and gaussian membrane curvature K_m align. k_{NP} is given as (3)

$$k_{NP} = \frac{1}{r_{NP}^{2}}$$

<div align="right">(2)</div>

And the gaussian curvature K_m is given as the product of the principal curvatures κ_1 and κ_2 (4)

$$K_m = \kappa_1 \kappa_2 = \frac{1}{r_1} \cdot \frac{1}{r_2}$$

<div align="right">(3)</div>

Ramanan *et al.* calculated gaussian curvature K_m profiles for clathrin-coated pits based on membrane deformation profiles modeled by Ramanan *et al.* (5). For early- and medium-stage clathrin-coated pits gaussian curvature K_m was found to range from 0.8 to $2.4 \cdot 10^{-3}$ nm^{-2}, which is in good correspondence with our nanoparticle's curvature k_{NP} of $0.8 \cdot 10^{-3}$ nm^{-2}, given by the hydrodynamic diameter d_h of our model system estimated via dynamic light scattering, in accordance with equation (2). Based on corresponding surface area values calculated by Agrawal *et al.* for clathrin-coated pits at early and medium stages of maturation (early: 1140 nm^2;

medium: 3760 nm^2) (6), we estimated δ to range from 0.07 to 0.23 (with O_{NP} = 16326 nm^2) for our nanoparticle model system binding into a pit.

As we consider the limits for $\delta \to 0$ (Eq. 4) and $\delta \to 1$ (Eq. 5) it is apparent that our expression is suitable to describe the number of ligand receptor pairs formed in dependence of the wrapping fraction δ. However, the introduction of this expression is only permissible if N_t is significantly higher than 1, so the addition of 1 in equation (1) resembling a single ligand binding regardless of the presence of membrane structures providing nanoparticles with a given wrapping fraction δ (e.g., CCPs) becomes negligible as δ increases (Eq. 5). This requirement can be considered given for most ligand-carrying nanostructures. It should also be noted that this mathematical consideration of the limiting cases of N in dependence of δ neglects the possibility of dissociation of the particle at low values of δ (in this case: $\lim_{\delta \to 0} N = 0$).

$$\lim_{\delta \to 0} N = 1 \tag{4}$$

$$\lim_{\delta \to 1} N \approx \delta N_t \quad \text{if } N_t \gg 1 \tag{5}$$

The absence of a given wrapping fraction corresponds to $A_m(K_m \approx k_{NP})$ = 0 within our model. Consequently, in this case δ = 0 (Eq. 1). Due to the correction of the particle valence N_t by δ the number of receptor-ligand bonds formed for the case a single particle results to be N = 1 (see equation 6 main text) and for the case of a particle number > 1 would be $[L]_{NP} = c_{NP}$ (this corresponds to the binding of one ligand per particle, see equation 7 in main text). In such a case nanoparticle binding is likely predominantly dictated by single ligand affinity and membrane bending energy as described by Bahrami et al. (7). In the presence of membrane structures possessing a curvature equal to nanoparticles curvature (e.g., CCPs), however, this membrane In the presence of a membrane structure with a curvature K_m corresponding to the curvature of the nanoparticles k_{NP} (e.g. CCPs), this membrane already has an area $A_m(K_m \approx k_{NP})$ > 0, which is available for the particles ahead of initial binding. This could also be referred to as a given wrapping fraction, in the sense that the particle already has a wrapping fraction δ > 0 at the time of initial binding.

Basic model for binding curve predictions. Considering the simplest case of linear receptor response (8), for the simple reaction equation given below, it can be assumed that the effect E triggered by ligand binding is proportional to the concentration [RL]. In addition, the maximum

3

effect E_{max} is proportional to the total number of receptors $[R_T]$, since $[R_T]$ is equal to $[RL]$ if all receptors are occupied.

$$L + R \rightleftarrows RL \rightarrow E$$
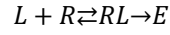
$$E \propto [RL] \qquad \text{and} \qquad E_{max} \propto [R_T]$$

Consequently, the degree of receptor occupation y can be expressed as follows.

$$y = \frac{[RL]}{[R_T]} = \frac{E}{E_{max}} \tag{6}$$

The concentration $[RL]$ can be expressed according to the law of mass action.

$$[RL] = \frac{[R_T] \cdot [L]}{K_D + [L]} \tag{7}$$

By transforming the law of mass action (Eq. 7) and inserting the derived expression for the degree of receptor occupation y (Eq. 6), we obtain an expression allowing us to predict binding curves for a ligand with a known dissociation constant K_D.

$$\frac{[RL]}{[R_T]} = \frac{E}{E_{max}} = \frac{[L]}{([L] + K_D)} \tag{8}$$

A necessary condition for this approach is a linear relationship between receptor occupancy $[RL]/[R_T]$ and the fractional response E/E_{max}.

$$\frac{[RL]}{[R_T]} \propto \frac{E}{E_{max}} \tag{9}$$

The relation $[RL]/[R_T] \propto E/E_{max}$ in equation (11) can be considered as given in case of the interaction of Ang II with the AT_1 receptor since the general prerequisites for the assumption of a linear response-receptor occupancy relation as pointed out by Buchwald (8) are met as 1. Ang II is known to act as a full agonist of AT_1R (9), 2. there occurs no Ca^{2+} signal amplification in the intracellular signal cascade of the AT1R (10,11), and 3. wild-type AT_1R exceeds no significant constitutive activity (12) regarding the $PLC-IP_3/Ca^{2+}$-signal pathway (13).

Using the expression for the δ-corrected nanoparticle valency N (Eq. 1), we introduced a modified expression for [L] allowing us to estimate the effective ligand concentration [L]$_{NP}$ as a function of the particle's molar concentration c_{NP}, the number of ligands attached to the nanoparticle N_t, and the wrapping fraction δ.

$$N_{NP} = c_{NP} N_A \tag{10}$$

$$[L]_{NP} = \frac{N_{NP}(N_t \delta + 1)}{N_A} \tag{11}$$

Here N_{NP} is the number of nanoparticles and N_A is Avogadro's constant. By inserting equation (10) for N_{NP} in equation (11), we yield a simplified expression for [L]$_{NP}$ given with equation (12).

$$[L]_{NP} = c_{NP}(N_t \delta + 1) \tag{12}$$

The effective ligand concentration [L]$_{NP}$ combined with the free ligand's dissociation constant K_D determined based on data obtained in the Ca^{2+} mobilization assays were employed to predict binding curves for a series of values for δ. To test the significance of our theoretical considerations regarding preferential nanoparticle binding to CCPs, we specifically predicted binding curves for the threshold values of δ (δ = 0.07-0.23) derived from the structural data of the CCPs (14,15). This allowed us to assess the overlay of experimental nanoparticle binding data and the derived expectation range for δ. The number of ligands attached to a single nanoparticle N_t was previously determined at ~2000 ligands per particle for the used nanoparticle model system (16).

$$\frac{E}{E_{max}} = \frac{c_{NP}(N_t \delta + 1)}{c_{NP}(N_t \delta + 1) + K_D} \tag{13}$$

Finally, equation (13) - obtained by inserting [L]$_{NP}$ (Eq. 12) for [L] in equation (8) - can be further modified by introducing a Hill-type extension as previously suggested by Buchwald (8) (Eq. 14). Since the Hill coefficient n is a solid measure for the degree of cooperativity α (17), this extension enables our model to account for cooperativity, thereby, significantly increasing its relevance considering multivalent interactions. Consequently, the integration of Hill coefficient values derived from curve fittings of our experimental data into the binding curve predictions resulted in a better overlap of experimental and predicted data.

$$\frac{E}{E_{max}} = \frac{\left(c_{NP}(N_t\delta + 1)\right)^n}{\left(c_{NP}(N_t\delta + 1)\right)^n + K_D{}^n}$$

(14)

For all predicted binding curves log EC_{50} was determined and compared with the values found for nanoparticle binding to untreated and 30 mM M-β-CD pretreated cells and for the free ligand Lys-Ang II. The residual sum of square (RSS) analysis showed that the curve predicted for δ = 0.10 using the model given in equation (14) had the highest overlap with the experimental data acquired for nanoparticle binding to untreated cells. Also, the found log EC_{50} for δ = 0.10 values aligned best. For M-β-CD pretreated cells on the other hand, the binding curve derived from experimental data laid between the predicted curves for δ of 0.01 and 0 (Fig. 6C).

Finally, the obtained best-fit value for δ was re-integrated into the standard binding saturation model (Eq. 15) modified to account for morphological correspondence δ by substituting the term $[L]_{NP}$ given in equation (12) for $[L]$. For E and E_{max} we inserted the change of Ca²⁺ level ΔCa^{2+} and maximum change of Ca²⁺ level ΔCa^{2+}_{max} to make the model applicable for data derived from Ca²⁺ mobilization assays.

$$\Delta Ca^{2+} = \Delta Ca^{2+}_{max} \frac{[L]_{NP}}{([L]_{NP} + K_D)}$$

(15)
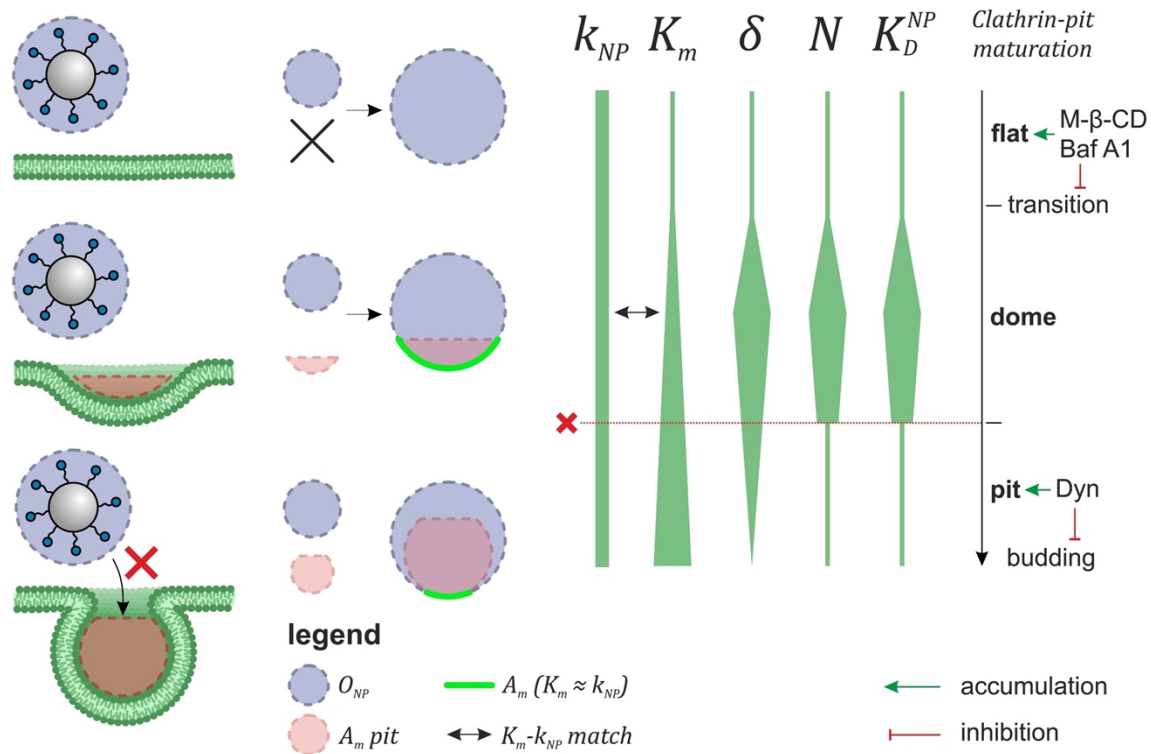
Figure S1. Preferential nanoparticle binding model applied to Bucher *et al.* maturation model We applied the introduced theoretical model on nanoparticle binding to the novel clathrin-coated pit maturation model recently introduced by Bucher *et al.* (18). According to their model, after the flat-dome-state transition, membrane curvature K_m continuously increases with ongoing maturation of the clathrin-coated pit. Applying this model to our theoretical nanoparticle binding model, it turns out that at a certain point in maturation, K_m coincides with the curvature of the nanoparticle k_{NP}. Consequently, at this point in maturation the wrapping fraction δ, the number of binding ligands N, and ultimately the nanoparticles avidity K_D^{NP} will peak. Again, after dome-pit-transition, the accessibility of the clathrin-coated pit for the nanoparticle is expected to be no longer given. All in all, these considerations suggest a preferential binding of ligand-functionalized nanoparticles to clathrin-coated pits in dome-state. We conclude from this that the choice of CCP maturation model does not affect the predictions of our theoretical model.
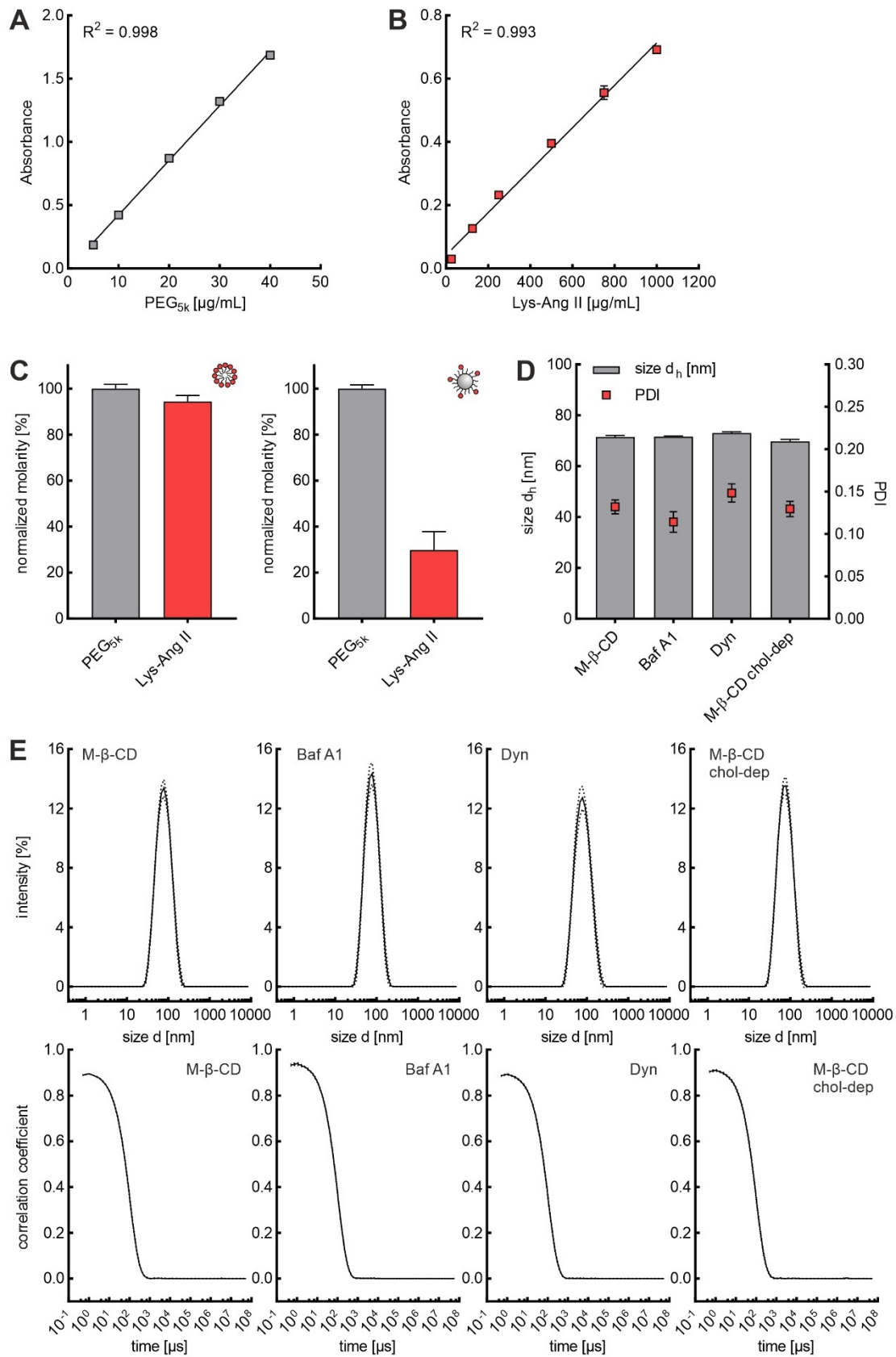
Figure S2. Characterization of Lys-Ang II modified PEG_{5k}-PLA_{10k} and NP_{Lys-Ang II} (A, B) Lys-Ang II coupled PEG_{5k}-PLA_{10k} polymer and functionalized nanoparticles were characterized using Pierce BCA assay and $BaCl_2$ based iodine assay to quantify Lys-Ang II and PEG molarity. Quantification was done via linear regression analysis conducted with serial dilutions of PEG_{5k} (40, 30, 20, 10, and 5 μg/mL) and Lys-Ang II (1000, 750, 500, 250, 125, and 25 μg/mL). (C) Coupling efficiency was quantified as the molar ratio of Lys-Ang II to PEG in Lys-Ang II-PEG-PLA micelles. For EDC/NHS-catalyzed Lys-Ang II functionalization of carboxy-PEG_{5k}-PLA_{10k} it was found to be 94.4 ± 2.7% (mean ± std.). Prepared nanoparticles were determined to carry 29.9 ± 9.0% (mean ± std.) Lys-Ang II ligand. (D) DLS characterization was done for each particle lot prepared for investigation of the three employed inhibitors M-β-CD, Baf A1, and Dyn. Hydrodynamic diameter d_h (z-average) was determined as 71.5 ± 0.5 (M-β-CD), 71.6 ± 0.2 (Baf A1), 73.1 ± 0.5 (Dyn), and 69.8 ± 0.5 (M-β-CD chol-dep). Polydispersity indices (PDI) were 0.13, 0.11, 0.15, and 0.13 (all error-bars reflect standard deviation). All data was derived from intensity-based distributions (E) DLS distribution curves and raw correlation data for each particle lot (dashed lines indicate std., N = 3).
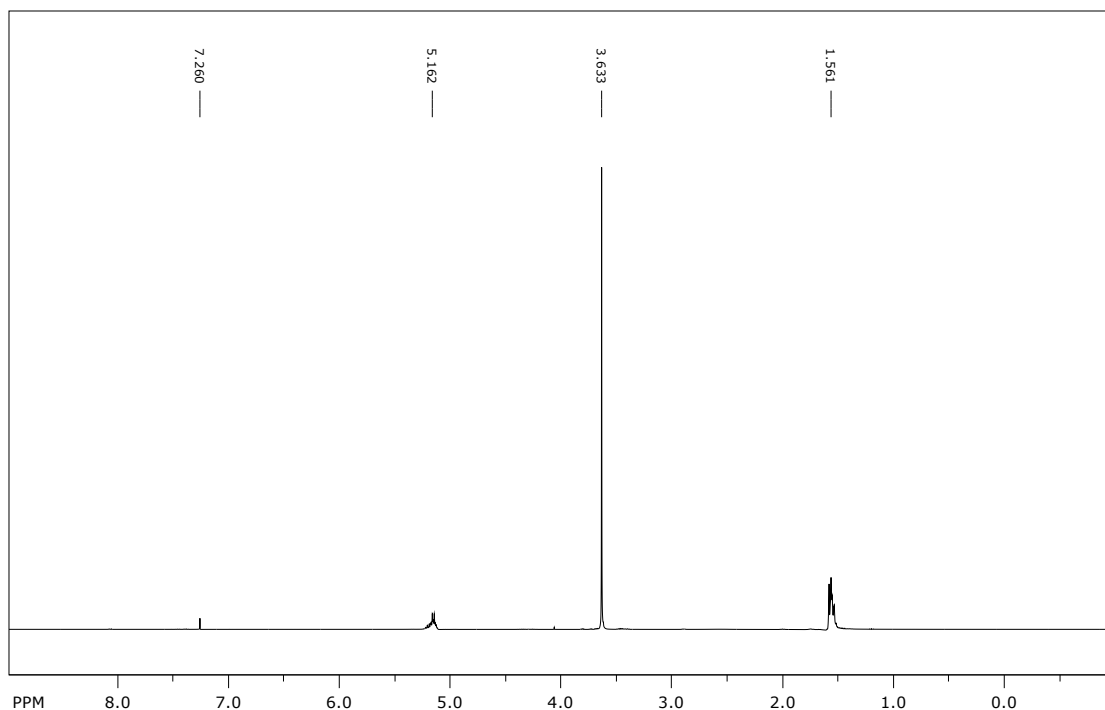
Figure S3. ^{1}H-NMR (CDCl_3, 400 MHz) of carboxy-PEG_{5k}-PLA_{10k} block copolymer. δ (ppm): 1.561 (-C(C**H**_3)H-, A_{PLA CH3} = 0.8514), 3.633 (-OC**H**_2C**H**_2-, A_{PEG} set to 1), 5.162 (-C(CH_3)**H**-, A_{PLA CH} = 0.2752), 7.260 (solvent peak).
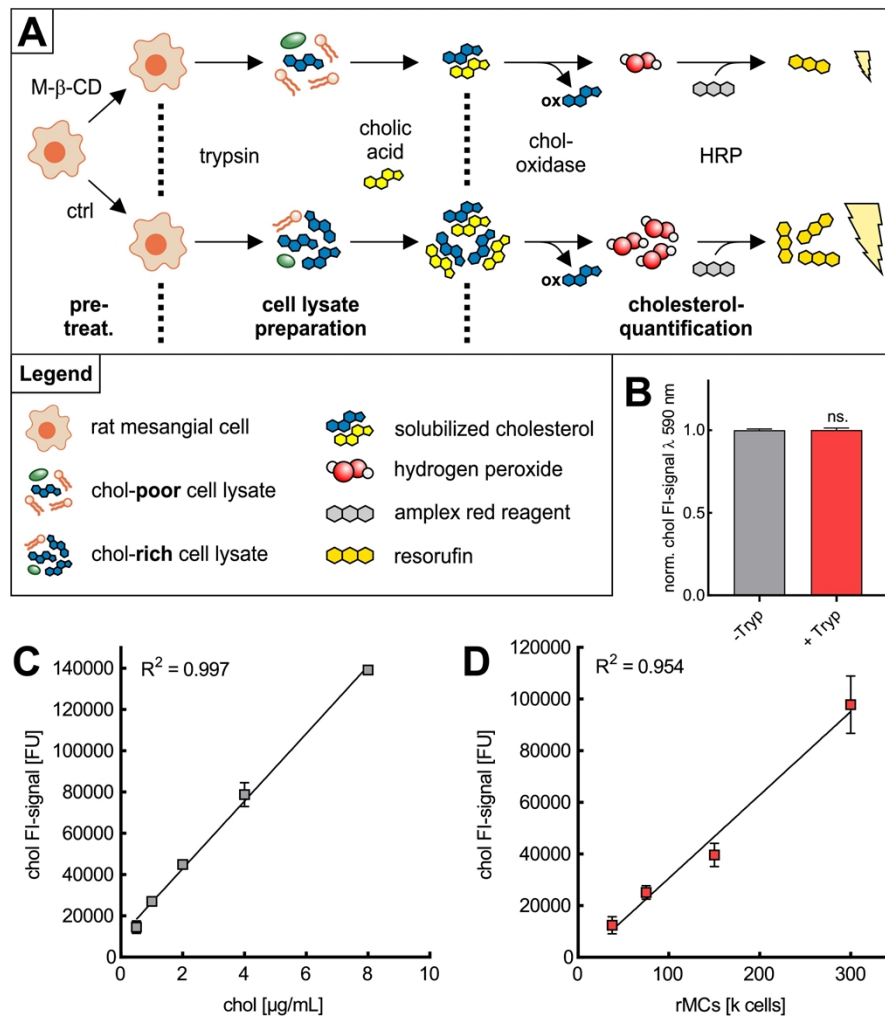
Figure S4. Cholesterol Quantification Assay (A) Scheme gives an overview about the sample preparation for Amplex™ Red-based cholesterol quantification assay. (B) Effect of possible residues of endopeptidase trypsin on the enzyme-stability of cholesterol oxidase (chol-oxidase) and horseradish peroxidase (HRP) was tested by performing the assay in presence and absence of 0.016% trypsin measuring 4 µg/mL cholesterol standard. Normalized fluorescence intensity detected was compared via un-paired two-tailed t-test (P = 0.729, t = 0.356, *df* = 10; ns. - not significant). (C) A serial dilution of cholesterol standard (8, 4, 2, 1, and 0.5 µg/mL) was prepared and measured (ex/em: 544/590 nm) on plate-reader to confirm linearity of obtained results and absence of significant background fluorescence. (D) To confirm linearity and absence of background fluorescence for cholesterol measurements in cells, cell pellets (300, 150, 75, and 37.5 k rMCs) were prepared and treated as shown in the scheme (for details refer to materials and methods section; all error-bars reflect standard deviation).
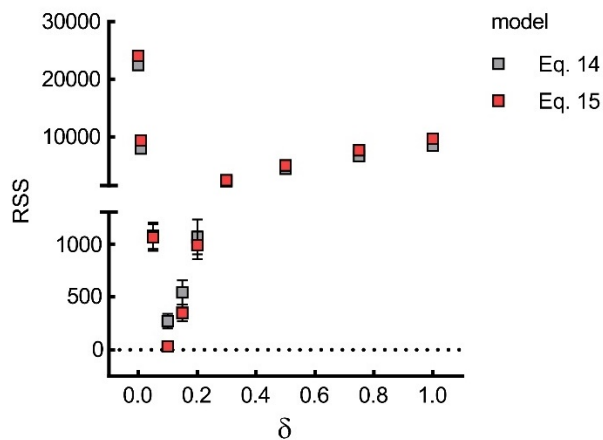
Figure S5. Residual sum of square analysis for binding curve models equation (13) and (14) To evaluate overlay of predicted binding curves with experimental data obtained in nanoparticle binding experiments, residual sum of square (RSS) values were plotted against δ. RSS values were determined for nanoparticle binding data against predicted data derived from basic binding curve model accounting for δ (Eq. 13) and binding curve model with Hill-extension (Eq. 14). Best overlay was found for δ = 0.10 employing binding curve model with Hill-extension (error-bars reflect standard deviation)

Table S1. Predicted Binding Data derived from δ-sensitive Model (Eq. 13) Data yielded from binding curve predictions employing basic δ-sensitive model (Eq. 13). [a]Dissociation constant K_D for free ligand Lys-Ang II was derived from saturation curve analysis using one-site specific binding model (see Quantification and Statistical Analysis).

c_{NP} [M]	N_t (14)	K_D [M] [a]	δ									
			0	0.01	0.05	0.10	0.15	0.20	0.30	0.50	0.75	1.0
			E/E_{max}									
1.00E-12			9.24E-6	1.94E-4	9.33E-4	1.85E-3	2.77E-3	3.69E-3	5.52E-3	9.17E-3	1.37E-2	1.82E-2
3.16E-12			2.92E-5	6.13E-4	2.94E-3	5.84E-3	8.72E-3	1.16E-2	1.73E-2	2.84E-2	4.20E-2	5.53E-2
1.00E-11			9.24E-5	1.94E-3	9.25E-3	1.82E-2	2.71E-2	3.57E-2	5.26E-2	8.47E-2	0.122	0.156
3.16E-11			2.92E-4	6.10E-3	2.87E-2	5.55E-2	8.09E-2	0.105	0.149	0.226	0.305	0.369
1.00E-10	~2000	1.08E-7	9.23E-4	1.90E-2	0.0854	0.157	0.218	0.270	0.357	0.481	0.581	0.649
3.16E-10			2.91E-3	5.78E-2	0.228	0.370	0.468	0.540	0.637	0.745	0.814	0.854
1.00E-9			9.16E-3	0.163	0.483	0.650	0.736	0.788	0.847	0.902	0.933	0.949
3.16E-9			2.84E-2	0.380	0.747	0.855	0.898	0.921	0.946	0.967	0.978	0.983
1.00E-8			8.46E-2	0.660	0.903	0.949	0.965	0.974	0.982	0.989	0.993	0.995

Table S2. Predicted Binding Data derived from δ-sensitive Model modified via Hill-extension (Eq. 14) Data yielded from binding curve predictions employing δ-sensitive model modified via Hill-extension (Eq. 14). [a]Dissociation constant K_D for free ligand Lys-Ang II was derived from saturation curve analysis using one-site specific binding model. [b]Hill-coefficient was derived from binding curve analysis of Ca^{2+} mobilization data obtained for Lys-Ang II functionalized nanoparticles employing four-parameter nonlinear regression model (see Quantification and Statistical Analysis).

				δ									
				0	0.01	0.05	0.10	0.15	0.20	0.30	0.50	0.75	1.0
c_{NP} [M]	N_t (14)	K_D [M] [a]	n [b]	E/E_{max}									
1.00E-12				3.93E-8	3.46E-6	3.49E-5	9.61E-5	1.74E-4	2.65E-4	4.81E-4	1.02E-3	1.85E-3	2.82E-3
3.16E-12				2.14E-7	1.88E-5	1.90E-4	5.22E-4	9.46E-4	1.44E-3	2.61E-3	5.51E-3	9.96E-3	1.51E-2
1.00E-11				1.16E-6	1.02E-4	1.03E-3	2.83E-3	5.12E-3	7.79E-3	1.40E-2	2.93E-2	5.19E-2	7.71E-2
3.16E-11				6.33E-6	5.57E-4	5.59E-3	1.52E-2	2.72E-2	4.09E-2	7.19E-2	0.141	0.229	0.312
1.00E-10	~2000	1.08E-7	1.47	3.44E-5	3.02E-3	2.96E-2	7.76E-2	0.132	0.188	0.296	0.471	0.618	0.712
3.16E-10				1.87E-4	1.62E-2	0.142	0.314	0.453	0.558	0.696	0.829	0.898	0.931
1.00E-9				1.02E-3	8.23E-2	0.475	0.713	0.818	0.873	0.926	0.963	0.980	0.987
3.16E-9				5.50E-3	0.328	0.831	0.931	0.961	0.974	0.985	0.993	0.996	0.997

| 1.00E-8 | | | | 2.92E-2 | 0.726 | 0.964 | 0.987 | 0.993 | 0.995 | 0.997 | 0.999 | 1.00 | 1.00 |

SI References

1. M Deserno, T Bickel, Wrapping of a spherical colloid by a fluid membrane. *Europhysics Letters (EPL)* **62**, 767–774 (2003).

2. J. Agudo-Canalejo, R. Lipowsky, Uniform and Janus-like nanoparticles in contact with vesicles: energy landscapes and curvature-induced forces. *Soft matter* **13**, 2155–2173 (2017).

3. A. Gray, E. Abbena, S. Salamon, *Modern differential geometry of curves and surfaces with Mathematica* (Chapman & Hall/CRC, 2006).

4. B. O'Neill, *Elementary differential geometry*, Elsevier Academic Press, Amsterdam, 2nd edn., 2006.

5. V. Ramanan, N. J. Agrawal, J. Liu, S. Engles, R. Toy, R. Radhakrishnan, Systems biology and physical biology of clathrin-mediated endocytosis. *Integrative biology : quantitative biosciences from nano to macro* **3**, 803–815 (2011).

6. N. J. Agrawal, J. Nukpezah, R. Radhakrishnan, Minimal mesoscale model for protein-mediated vesiculation in clathrin-dependent endocytosis. *PLoS computational biology* **6**, e1000926 (2010).

7. A. H. Bahrami, R. Lipowsky, T. R. Weikl, The role of membrane curvature for the wrapping of nanoparticles. *Soft matter* **12**, 581–587 (2016).

8. P. Buchwald, A single unified model for fitting simple to complex receptor response data. *Scientific reports* **10**, 13386 (2020).

9. Y. H. Feng, K. Noda, Y. Saad, X. P. Liu, A. Husain, S. S. Karnik, The docking of Arg2 of angiotensin II with Asp281 of AT1 receptor is essential for full agonism. *The Journal of biological chemistry* **270**, 12846–12850 (1995).

10. S. J. Forrester, G. W. Booz, C. D. Sigmund, T. M. Coffman, T. Kawai, V. Rizzo, R. Scalia, S. Eguchi, Angiotensin II Signal Transduction: An Update on Mechanisms of Physiology and Pathophysiology. *Physiological reviews* **98**, 1627–1738 (2018).

11. M. de Gasparo, K. J. Catt, T. Inagami, J. W. Wright, T. Unger, International union of pharmacology. XXIII. The angiotensin II receptors. *Pharmacological reviews* **52**, 415–472 (2000).

12. D. Hoyer, E. P. Zorrilla, P. Cottone, S. Parylak, M. Morelli, N. Simola, J. D. Lane, M. M. Morgan, M. J. Christie, C. J. Hillard, A. J. Budney, R. G. Vandrey, T. Robbins, P. Nencini, M. S. Milella, N. Mirza, V. L. Harvey, T. Dickenson, S. Miyamoto, O. Almeida, N. Sousa, S. Yu, A. Absalom, D. Menon, P. L. Delgado, C. Höschl, T. L. White, R. Depue, C. Baltes, T. Mueggler, M. Rudin, P. J. Flor, I. Neumann, C. A. Erickson, D. J. Posey, K. Blankenship, K. A. Stigler, C. J. McDougle, E. Sibille, N. Edgar, M. Lader, T. Duka, E.

Childs, B. Hahn, J. Harro, P. Newhouse, H. Wilkins, Y. Alici, W. Breitbart, E. Nestler, A. R. Isles, L. Wilkinson, S. Pandey, S. G. Siris, P. Willner, M. Billiard, B. Lemmer, J.-M. Scherrmann, L. H. Price, T. J. Banasikowski, R. J. Beninger, J. Harvey, B. E. Leonard, K. Wolff, A. Padhi, N. Fineberg, W. H. Meck, C. V. Buhushi, L. R. McMahon, Y. Chudasama, M. Kuhar, J. D. Uys, P. W. Kalivas, M. Shoaib, D. Bertrand, H. Rollema, R. S. Hurst, M. Bloch, J. F. Leckman, B. J. Sahakian, S. Morein-Zamir, A. Jackson, B. J. Harrison, C. Pantelis, I. Hindmarch, A. J. Bond, J. M. Monti, D. R. Christensen, W. K. Bickel, M. J. Bubar, K. A. Cunningham, C. A. Franco, M. Potenza, M.-I. López-Ibor, J. J. López-Ibor, J. H. Friedman, A. Hofer, M. I. Palmatier, R. A. Bevins, T. Tzschentke, D. Roberts, S. Anagnostaras, J. R. Sage, S. A. Carmack, S. J. Kohut, A. L. Riley, R. F. Mucha, J. Prickaerts, O. Stiedl, S. O. Ögren, K. Nader, O. Hardt, P. V. Migues, A. Christopoulos, G. D. Stewart, P. M. Sexton, Y. Shaham, S. G. Nair, S. H. Heil, S. C. Sigmon, S. T. Higgins, M. N. Branch, M. Cain, M. T. Bardo, R. L. Balster, S. Walsh, R. de Rijk, R. de Kloet, C. H. Bourke, M. J. Owens, C. Viollet, J. Epelbaum, K. Mann, F. Kiefer, M. Owens, C. Bourke, H. McAllister-Williams, A. Marneros, R. Andrade, I. Izquierdo, L. R. M. Bevilaqua, M. Cammarota, C. Hiemke, M. I. Colado, R. Green, "Constitutive Activity" in Encyclopedia of Psychopharmacology, I. P. Stolerman, Ed. (Springer Berlin Heidelberg, 2010), p. 349.

13. M. Auger-Messier, G. Arguin, B. Chaloux, R. Leduc, E. Escher, G. Guillemette, Down-regulation of inositol 1,4,5-trisphosphate receptor in cells stably expressing the constitutively active angiotensin II N111G-AT(1) receptor. *Molecular endocrinology (Baltimore, Md.)* **18**, 2967–2980 (2004).

14. A. E. Nel, L. Mädler, D. Velegol, T. Xia, E. M. V. Hoek, P. Somasundaran, F. Klaessig, V. Castranova, M. Thompson, Understanding biophysicochemical interactions at the nano-bio interface. *Nature materials* **8**, 543–557 (2009).

15. N. Hoshyar, S. Gray, H. Han, G. Bao, The effect of nanoparticle size on in vivo pharmacokinetics and cellular interaction. *Nanomedicine (London, England)* **11**, 673–692 (2016).

16. S. Maslanka Figueroa, D. Fleischmann, S. Beck, A. Goepferich, The Effect of Ligand Mobility on the Cellular Interaction of Multivalent Nanoparticles. *Macromolecular bioscience*. 10.1002/mabi.201900427, e1900427 (2020).

17. C. A. Hunter, H. L. Anderson, What is cooperativity? *Angewandte Chemie International Edition* **48**, 7488–7499 (2009).

18. D. Bucher, F. Frey, K. A. Sochacki, S. Kummer, J.-P. Bergeest, W. J. Godinez, H.-G. Kräusslich, K. Rohr, J. W. Taraska, U. S. Schwarz, S. Boulant, Clathrin-adaptor ratio and membrane tension regulate the flat-to-curved transition of the clathrin coat during endocytosis. *Nature communications* **9**, 1109 (2018).